Journal of Agricultural Science; Vol. 5, No. 8; 2013
ISSN 1916-9752 E-ISSN 1916-9760
Published by Canadian Center of Science and Education

Influence of Tyre Inflation Pressure and Wheel Load on the Traction Performance of a 65 kW MFWD Tractor on a Cohesive Soil

Andrea Battiato[1,2] & Etienne Diserens[1]

[1] Agroscope Reckenholz-Tänikon Research Station ART, Ettenhausen, Switzerland

[2] Department of Land, Environment, Agriculture and Forestry L.E.A.F., University of Padua, Legnaro, Italy

Correspondence: Andrea Battiato, Agroscope Reckenholz-Tänikon Research Station ART, CH-8356 Ettenhausen, Switzerland. E-mail: andrea.battiato@agroscope.admin.ch, andrea.battiato@studenti.unipd.it

Received: May 15, 2013 Accepted: June 18, 2013 Online Published: July 15, 2013

doi:10.5539/jas.v5n8p197 URL: http://dx.doi.org/10.5539/jas.v5n8p197

Abstract

The choice of tractor configuration is of primary importance in tillage operations for the optimisation of traction performance, i.e. for limiting slip which involves energy loss. To a great extent, this aspect affects the fuel consumption and the time required for soil tillage. Tyre inflation pressure and wheel load are both easily managed parameters which play a significant role in controlling the traction performance of a tractor. The present study aimed to investigate the influence of tyre inflation pressure and wheel load on the traction performance of a mechanical front wheel drive MFWD tractor (65 kW engine power) on an agricultural clay (C) Vertic Cambisol on the basis of results of traction tests and simulations with a semi-empirical soil-tyre interaction model adapted for MFWD vehicles. The traction tests were carried out using four tractor configurations with two tractor weights (40.8 kN and 50.2 kN) and two tyre inflation pressures (60 kPa and 160 kPa). Traction performance was considered in terms of drawbar pull, traction coefficient, tractive efficiency, power delivery efficiency and specific fuel consumption in relation to wheel slip. A decrease in tyre pressure and an increase in wheel load resulted in higher drawbar pull however, only the former produced improvements in terms of coefficient of traction, tractive efficiency, power delivery efficiency and specific fuel consumption, while the only significant benefit resulting from the latter was a reduction in specific fuel consumption at a tyre pressure of 160 kPa and a slip of under 15%.

Keywords: soil-tyre interaction, traction performance, tractive efficiency, power delivery efficiency, specific fuel consumption

Nomenclature

a	Parameter of the parabolic equation which defines the shape of the contact surface (m^{-1})
A	Fitting parameter for the power delivery efficiency as a function of wheel slip
B	Fitting parameter for the specific fuel consumption as a function of wheel slip (kW h g^{-1})
b	Contact patch smaller dimension (width of the tyre) (m)
c	Soil cohesion (kPa)
ds	Infinitesimal area of the soil-tyre contact surface (m^2)
DP	Drawbar pull (kN)
D_{rim}	Rim diameter (m)
e_t	Eccentricity of the vertical soil reaction relative to the rear point of the contact surface (m)
e_0	Eccentricity of the centre of the wheel relative to the rear point of the contact surface (m)
FC	Gravimetric fuel consumption (kg h^{-1})
GT	Gross traction (kN)
h	Height of the drawbar (m)
i	Wheel slip
j	Soil shear displacement (m)
k	Soil shear deformation modulus (m)
$K_{c,f}$	Soil cohesive modulus of deformation for the front wheel (kN $m^{-(n+1)}$)
$K_{c,r}$	Soil cohesive modulus of deformation for the rear wheel (kN $m^{-(n+1)}$)
K_{carc}	Tyre carcass stiffness (kN m^{-1})
K_s	Theoretical speed ratio

K_v	Coefficient of vertical stiffness of the tyre for unit length of the contact surface (kN m^{-2})
$K_{\varphi,f}$	Soil frictional modulus of deformation for the front wheel (kN m$^{-(n+2)}$)
$K_{\varphi,r}$	Soil frictional modulus of deformation for the rear wheel (kN m$^{-(n+2)}$)
l_A	Fitting parameter for the power delivery efficiency as a function of wheel slip
l_B	Fitting parameter for the specific fuel consumption as a function of wheel slip
L	Wheelbase of the tractor (m)
M_{GT}	Driving torque relative to the gross traction (kN m)
M_r	Resistance moment due to eccentricity of the vertical soil reaction respect to the wheel centre (kN m)
n_f	Exponent of soil deformation for the front wheel
n_r	Exponent of soil deformation for the rear wheel
NT	Net traction (kN)
p_h	Horizontal component of the elementary force at soil-tyre contact surface (kN)
p_s	Vertical soil pressure (kPa)
p_v	Vertical component of the elementary force at soil-tyre contact surface (kN)
P_{in}	Tyre inflation pressure (kPa)
PTO	Power-take-off (kW)
R	Unloaded radius of the wheel (m)
R_c	Soil compaction resistance (kN)
R_{GT}	Distance from the centre of the wheel to the point of application of the gross traction (m)
R_r	Rolling radius of the wheel (m)
SFC	Specific fuel consumption (kg kW^{-1} h^{-1})
T	Total driving torque on the wheel (kN m)
V_a	Actual forward velocity of the wheel (m s^{-1})
W	Vertical component of the total soil reaction / wheel load (kN)
$W_{tractor}$	Tractor weight (kN)
W_0	Wheel load in stationary condition (kN)
x	Horizontal coordinate (m)
x_0	Length of the soil-tyre contact surface in the horizontal direction (m)
z	Vertical coordinate (soil sinkage) (m)
z_0	Rut depth (m)

Greek letters

α	Angle between the tangent to the infinitesimal area of the soil-tyre contact and the x-axis (°)
δ	Tyre vertical deflection (m)
ΔK_p	Inflation pressure dependence of the tyre (kN m^{-1} kPa^{-1})
η_{PD}	Power delivery efficiency
η_{tr}	Tractive efficiency
θ_A	Fitting parameter for the power delivery efficiency as a function of wheel slip
θ_B	Fitting parameter for the specific fuel consumption as a function of wheel slip
μ_{tr}	Traction coefficient
σ	Normal stress at soil-tyre contact surface (kPa)
σ_v	Vertical component of the surface traction (kPa)
τ	Shear stress at soil-tyre contact surface (kPa)
τ_{max}	Soil strength (kPa)
φ	Angle of soil shear resistance (°)
ω	Angular velocity of the wheel (s^{-1})

1. Introduction

Since the traction performance of a tractor has a major impact on both fuel consumption and the time required for soil tillage, optimising this performance is clearly of crucial importance in tillage management.

Traction performance is usually expressed in terms of the pulling force available at the tractor drawbar (drawbar pull), or alternatively in terms of the traction coefficient μ_{tr}, which is defined as the drawbar pull DP to tractor weight $W_{tractor}$ ratio:

$$\mu_{tr} = \frac{DP}{W_{tractor}} \tag{1}$$

Other important parameters involving the energy aspects of traction performance are tractive efficiency η_{tr} and power delivery efficiency η_{PD}. The tractive efficiency of a drive wheel is defined as:

$$\eta_{tr} = \frac{NT\,V_a}{T\omega} \tag{2}$$

which expresses the ratio of output power to input power of the wheel, NT being the net traction force, V_a the actual forward velocity of the wheel, T the total driving torque on the wheel, and ω the angular velocity of the wheel. The same tractive efficiency can be defined for the tractor as:

$$\eta_{tr} = \frac{DP\,V_a}{\sum T\omega} \tag{3}$$

and represents the fraction of power delivered to the tractor wheels that is available as drawbar power. Servadio (2010) considered both the traction coefficient and the tractive efficiency to characterise field performance of several wheeled and tracked vehicles in central Italy.

Power delivery efficiency is defined as the ratio of delivered tractive power (drawbar power) to tractor input power from the engine, and represents the fraction of power produced by the engine of a tractor that is available as tractive power (Shell, Zoz, & Turner, 1997; Turner, Shell, & Zoz, 1997). In order to consider the engine power input, the equivalent *PTO* (power-take-off) power can be used (Zoz, Turner, & Shell, 2002), in which case the power delivery efficiency can be defined as:

$$\eta_{PD} = \frac{DP\,V_a}{Equivalent\ PTO\ power} \tag{4}$$

In terms of fuel consumption, a parameter related to the traction performance of the tractor is the specific fuel consumption *SFC*, defined as the ratio of the fuel consumption expressed in kg h^{-1} (gravimetric) or l h^{-1} (volumetric) to the engine power input, or alternatively to the drawbar power.

The traction performance of a wheeled tractor is the result of a stress-strain interaction between the tractor wheels and the topsoil. This interaction is affected by several factors, including the mechanical behaviour of the topsoil, power and geometry (wheelbase and drawbar height) of the tractor, number of drive wheels, wheel load, wheel slip, tyre dimensions (width and diameter), tyre inflation pressure and stiffness, all of which exert a significant influence. While most of the above factors are more or less constrained, wheel load and tyre inflation pressure can be varied within wide ranges, allowing easy management of the traction performance of the tractor. Consequently, these factors are highly advantageous for practical applications. The influence of wheel load and tyre inflation pressure on tractor traction performance has been investigated using both a theoretical and an experimental approach.

With regard to the former approach, the semi-empirical models of interaction between soil and a pneumatic wheel based on Bekker's theory (Bekker, 1960) offer a valid framework for the better understanding and simulation of the effects of both tyre inflation pressure and wheel load on the traction performance of the tractor-soil system. In this context several approaches have been presented assuming the contact surface between soil and tyre to be a combination of a flattened portion and the unloaded contour (Bekker, 1960; Wong, 1989), or as an arc of an equivalent rigid wheel of larger diameter (Fujimoto, 1977), or also described as a parabolic configuration with its apex at the front point of contact (Schmid, 1995). More recently, Shmulevich and Osetinsky proposed a model based on a parabolic soil-tyre contact surface with its apex at the rear point of contact (Shmulevich & Osetinsky, 2003; Osetinsky & Shmulevich, 2004), which presents a simple mathematical treatment and allows a reliable simulation of traction performance.

With regard to the latter approach, many authors have reported experimental results showing some benefits of reduced tyre inflation pressure for tractor traction performance (Zombori, 1967; Gee-Clough, McAllister, & Evernden, 1977; Burt & Bailey, 1982; Turner, 1993; Zoz & Grisso, 2003). Whilst evident for radial-ply tyres, these benefits in some cases turned out to be less or not at all significant for bias-ply tyres (Lee & Kim, 1997). Serrano, Peça, Silva, and Márquez (2009) studied the performance of a tractor (59 kW engine power) with two static ballasts, with and without liquid tyre ballast, and at three different inflation pressures. The use of liquid ballast in the tyres turned out not to improve work-rate and besides to increase fuel consumption per hectare of 5-10%. The use of higher tyre inflation pressures produced a slight reduction in work-rate (3-5%) with a large

increase in fuel consumption per hectare (10-25%). Burt, Balley, Patterson, & Taylor (1979) investigated the influence of dynamic wheel load on tractive efficiency on both a compacted and an uncompacted soil, observing that, with constant travel reduction (slip), an increase in dynamic load produced in the former case an increase and in the latter case a decrease in tractive efficiency. Charles (1984) carried out tractor-traction tests on a low-plasticity silt soil in both a tilled (soft) and firm condition at different static loads and tyre inflation pressures. His findings show that both an increase in static load and a decrease in tyre pressure resulted in higher traction performance in terms of drawbar pull and tractive efficiency for both of the soil conditions considered. Lyne, Burt, and Meiring (1984) reported results of traction tests with a 4WD tractor on a Westleigh clay in two soil conditions and with several combinations of static load and tyre pressure, showing that as static load increased at each inflation pressure, so did drawbar pull, drawbar power and power demand on the engine, with a corresponding decrease in specific fuel consumption (drawbar power basis). According to results reported by Turner (1993) and Zoz and Grisso (2003), an increase in tractor weight (wheel load), obtained with ballasts and tyre inflation pressure adapted to the weight, makes for higher drawbar pull, although it does not seem to result in a significant variation in terms of traction coefficient or power delivery efficiency. Results of traction tests reported by Zoz and Grisso (2003) for a single 520/85R46 radial tyre with inflation pressure adapted for different wheel loads showed a negligible influence on maximum tractive efficiency. Burt, Lyne, Meiring, and Keen (1983) and Burt and Bailey (1982) showed how, for a given drawbar pull, the tractive efficiency of both radial-ply and bias-ply tyres can be maximised by selecting proper levels of dynamic load and inflation pressure. Lyne et al. (1984) also pointed out the importance of an appropriate choice of both dynamic load and tyre inflation pressure in order to optimise the tractive efficiency of a tractor. Moreover, it was observed that operating at optimum tractive efficiency allows minimum specific fuel consumption (Lyne et al., 1984; Jenane, Bashford, & Monroe, 1996). Gee-Clough, Pearson, and McAllister (1982) demonstrated the key role of a wheel load properly matched to tractor power, speed, and drawbar pull at low tyre inflation pressure (110 kPa or less), in the optimisation of the power output of wheeled tractors in frictional-cohesive soils. This variety of studies has produced results which in some cases appear to contradict one another. It should be pointed out, however, that the widely differing experimental conditions considered (soil and tyre types, wheel load range, tyre pressure range) make it difficult to draw proper comparisons, as do the different layouts and methodologies used for the traction tests.

In this context, the issue of improving traction performance of a tractor by ballasting or by reducing the inflation pressure of the tyres is thought to require further and deeper understanding in order to better define clear indications for a correct choice of the tractor configuration, this latter considerably contributing in more appropriate tillage management. Furthermore, some of the studies presented either dealt with big tractors (Turner, 1993; Zoz & Grisso, 2003) or the single wheel testers (Burt et al., 1979; Burt & Bailey, 1982; Gee-Clough et al., 1977), whilst the performance of medium powered tractors, which are reasonably widespread in Central Europe, has received less attention.

In this paper, the influence of tyre inflation pressure and wheel load on the traction performance of a MFWD tractor (65 kW engine power) on an agricultural clay (C) Vertic Cambisol is compared and discussed on the basis of results of field traction tests as well as simulations with a semi-empirical soil-tyre interaction model adapted for MFWD vehicles, with a mechanistic interpretation of results. In addition, two equations describing the relationships power delivery efficiency-wheel slip and specific fuel consumption-wheel slip are presented.

2. Materials and Methods

2.1 Soil-Tyre Interaction Modelling

Forces acting on the driven pneumatic wheel with a detail of the elementary forces acting at soil-tyre contact according to Shmulevich and Osetinsky (2003) are shown in Figure 1.

The following assumptions are considered: the soil behaves as a plastic non-linear medium, the wheel rolls in steady-state motion at a low velocity, tyre deformations are linear elastic, the wheel-soil interaction is two dimensional (plane-strain approach). This latter assumption implies that the rut depth is the same across the width, and the width is the same along the contact surface, moreover all values are referred to the unit width of the wheel.

According to Bekker's theory, the vertical soil pressure along the soil-tyre contact surface is assumed to be equal to the soil pressure beneath the compression plate of a bevameter at the same depth:

$$p_s = \left(\frac{K_c}{b} + K_\varphi \right) z^n \tag{5}$$

wherein p_s is the vertical soil pressure under the plate, z is the soil sinkage, n is the exponent of deformation, and b is the smaller dimension of the contact patch (width of the tyre), whilst K_c and K_φ are the cohesive and frictional

modulus of soil deformation, respectively.

The vertical component of the total soil reaction must balance out the wheel load W, this condition is expressed as follows:

$$W = \int_0^{x_0} p_s b dx \tag{6}$$

wherein x_0 is the maximum value of the horizontal coordinate according to Figure 1.

The equation of the parabolic contact surface (Osetinsky & Shmulevich, 2004) expresses the sinkage z as a function of the horizontal coordinate x:

$$z = z_0 - ax^2 \tag{7}$$

z_0 being the rut depth and a being the parameter of the parabolic equation.

Integral 6 is solved by means of a series expansion of function 7 limited to the second term, similarly to the approach reported by Wong (2008). This results in:

$$W = \frac{K_c + bK_\varphi}{3} z_0^n \sqrt{\frac{z_0}{a}} (3-n) \tag{8}$$

Tyre stiffness is defined according to Lines and Murphy (1991) as the sum of two components, the carcass stiffness K_{carc} and the product $\Delta K_p P_{in}$, where ΔK_p is the inflation pressure dependence of the tyre and P_{in} is the inflation pressure. Consequently, the stiffness has both a constant component and a component which varies with the inflation pressure.

The same equilibrium condition in equation 6 can be expressed in terms of the tyre stress state according to its stress-deflection relationship:

$$W = K_v \left\{ \frac{a x_0^3}{3} - \sqrt{R^2 - e_0^2} \left(x_0 - \frac{e_0}{2} \right) + \frac{x_0 - e_0}{2} \sqrt{R^2 - (x_0 - e_0)^2} + \frac{R^2}{2} \left[arcsin\left(\frac{x_0 - e_0}{R} \right) + arcsin\left(\frac{e_0}{R} \right) \right] \right\} \tag{9}$$

where e_0 is the eccentricity of the centre of the wheel relative to the rear point of the contact surface (Figure 1), R is the unloaded radius of the wheel, and K_v is the coefficient of vertical stiffness of the tyre for unit length of contact surface, which can be expressed as a function of K_{carc} and the product $\Delta K_p P_{in}$:

$$K_v = \frac{W}{R^2 \, arcsin\left(\frac{x_0}{2R} \right) - \frac{x_0}{2} \left(R - \frac{W}{K_{carc} + \Delta K_p P_{in}} \right)} \tag{10}$$

A detailed derivation of equation 9 is described in Osetinsky and Shmulevich (2004).

Rut depth z_0 and the parameter a which define the soil-tyre contact surface are determined by simultaneously solving equations 8 and 9.

The horizontal component of the elementary force p_h and the vertical component of the elementary force p_v acting at soil-tyre contact are given by:

$$p_h = (\sigma ds) sin\alpha - (\tau ds) cos\alpha \tag{11}$$

$$p_v = (\sigma ds) cos\alpha + (\tau ds) sin\alpha \tag{12}$$

where ds is the infinitesimal area of the contact surface and α is the angle between the tangent to the infinitesimal area of the soil-tyre contact surface and the x-axis (Figure 1), whilst σ and τ are the normal stress and the tangential stress at the soil-tyre contact surface, respectively. Moreover, it turns out that (Figure 1):

$$ds \, sin\alpha = bdz \tag{13}$$

and

$$ds \, cos\alpha = bdx \tag{14}$$

The shear stress τ at each point of the contact surface depends on the normal stress σ, the soil cohesion c, the angle of soil shear resistance φ, the soil shear deformation modulus k, and the soil shear displacement j along the contact surface. This dependence is described by the well known equation proposed by Janosi and Hanamoto (1961):

$$\tau = \left(c + \sigma \tan\varphi\right)\left(1 - e^{-j/k}\right) \tag{15}$$

The soil shear displacement at each point of the contact surface is calculated by integrating the component of the absolute velocity tangent to the surface (slip velocity) over time, similarly to the approach described by Wong and Reece (1967) for a rigid wheel. The calculation of the soil shear displacement is described in detail in Osetinsky and Shmulevich (2004) and yields the following integral to be solved by a numerical approach:

$$j = \int_{x}^{x_0} \frac{\left[ax\left(x-2e_0\right)+\sqrt{R^2-e_0^2}-\frac{V_a}{\omega}\right]\left[ax\left(x-2e_0\right)+\sqrt{R^2-e_0^2}\right]}{\sqrt{1+\left(2ax\right)^2}\left[\left(ax^2-\sqrt{R^2-e_0^2}\right)^2+\left(x-e_0\right)^2\right]}dx \tag{16}$$

In integral 16, V_a is the actual forward velocity of the wheel, whilst ω is the angular velocity of the wheel. The wheel slip i relates the actual forward velocity and the angular velocity of the wheel:

$$i = \frac{\omega R_r - V_a}{\omega R_r} \tag{17}$$

where R_r is the rolling radius of the wheel.

The normal stress at each point of the contact surface is given by:

$$\sigma = \frac{\sigma_v - c\left(1-e^{-j/k}\right)2ax}{1+tg\varphi\left(1-e^{-j/k}\right)2ax} \tag{18}$$

wherein σ_v is the vertical component of the surface traction, defined as:

$$\sigma_v = \frac{p_v}{bdx} = \frac{K_v\delta}{b} \tag{19}$$

where δ is the vertical tyre deflection at each point of the contact surface (Figure 1) which can be defined on the basis of the geometry of the contact surface as:

$$\delta = \sqrt{R^2-\left(x-e_0\right)^2}-\sqrt{R^2-e_0^2}+ax^2 \tag{20}$$

The gross traction GT is obtained by using a numerical approach to integrate the horizontal components p_h of the elementary force over the contact surface. According to equations 11, 13, 14, 15 and 18 this condition is defined as:

$$GT = \int_{x}^{x_0} \frac{\sigma_v\left[2ax-\tan\varphi\left(1-e^{-j/k}\right)\right]-c\left(1-e^{-j/k}\right)\left(2ax\right)^2+1}{1+2ax\left(1-e^{-j/k}\right)\tan\varphi}bdx \tag{21}$$

The main resisting forces acting on a tractor moving on a flat terrain are represented by the internal resistance of the running gear and the resistance due to the interaction with the terrain. Since the latter factor is, to a great extent, the most significant (Bekker, 1960; Wong, 2008), the internal resistance can be neglected, at least in the first approximation. The resistance due to interaction with the terrain, according to Figure 1, corresponds to the soil compaction resistance R_c. Additional soil bulldozing resistance must be taken into account in soft soils where wheel sinkage is significant. In the cases considered here, the bulldozing effect may be reliably expected not to occur because of the limited wheel sinkage values. The soil compaction resistance is calculated as the vertical work performed in making a rut of a depth z_0 (Bekker, 1960):

$$R_c = \left(K_c + bK_\varphi\right)\frac{z_0^{n+1}}{n+1} \tag{22}$$

The net traction NT is finally calculated as:

$$NT = GT - R_c \tag{23}$$

According to Figure 1, the total driving torque T on the wheel is calculated as:

$$T = M_{GT} + M_r \tag{24}$$

The term M_{GT} is the driving torque relative to the gross traction GT, which is given by:

$$M_{GT} = GT\ R_{GT} \tag{25}$$

where R_{GT} is the distance from the centre of the wheel to the point of application of the gross traction (Figure 1), calculated as described in Osetinsky and Shmulevich (2004).

The term M_r is the resistance moment due to the eccentricity of the vertical soil reaction with respect to the wheel centre on which the wheel load is applied (Figure 1):

$$M_r = W(e_t - e_0) \tag{26}$$

The eccentricity relative to the rear point of the soil-tyre contact surface e_t is calculated from the equilibrium of the moving wheel, according to the original model (Osetinsky & Shmulevich, 2004).

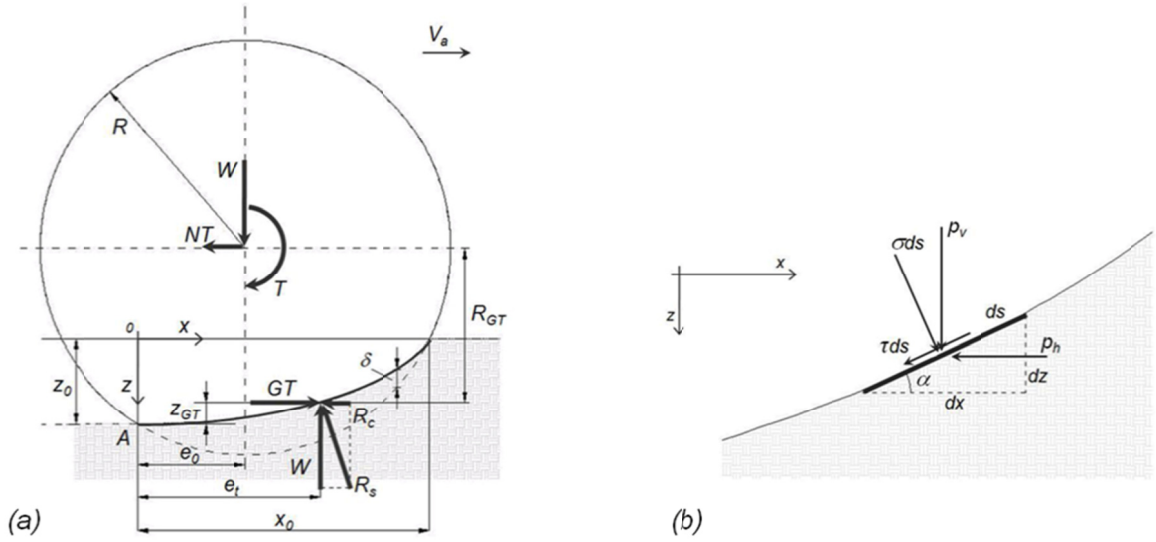

Figure 1. Interaction between soil and a driven pneumatic wheel *(a)*, with the detail of the elementary forces acting at the soil-tyre contact surface *(b)*, according to Shmulevich and Osetinsky (2003)

2.2 Traction Performance of a MFWD Tractor Modelling

The soil-tyre interaction model was adapted to a MFWD tractor by considering the multipass effect, the dynamic wheel load due to the load transfer effect and the theoretical speed ratio K_s which controls the ratio between the slip of the front wheel i_{front} and the rear wheel i_{rear} of a MFWD tractor in straight line motion with rigid coupling between the front and the rear axles.

The multipass effect was considered by means of a differentiated mechanical characterisation of soil interacting with the front and rear wheel, respectively. Soil parameters were derived with bevameter tests before tractor passage as well as on the rut left from the passage of the front wheel, according to Bekker (1960).

When the net traction force is developed, the distribution of the tractor load between the front and rear axles differs from that of the stationary state owing to the transfer of load towards the rear axle. Such an effect is referred to as the load transfer effect, and causes the rear axle load to rise when net traction increases, with an opposite effect on the front axle. The dynamic wheel load was determined on the basis of the equilibrium condition of the tractor body (Figure 2), as follows:

$$W_f = W_{0,f} - \Delta W \tag{27}$$

for the front wheel, and

$$W_r = W_{0,r} + \Delta W \tag{28}$$

for the rear wheel.

The terms $W_{0,f}$ and $W_{0,r}$ represent the stationary wheel loads on the front and rear wheel, respectively, whilst W_f and W_r are the wheel loads in dynamic conditions on the front and rear wheel, respectively. The term ΔW represents the difference between the wheel load in a stationary and a dynamic condition owing to the load transfer effect. According to Figure 2 ΔW is calculated as:

$$\Delta W = \frac{T_f + T_r + \left(NT_f + NT_r\right)\left(h - R_{r,r}\right) + NT_f\left(R_{r,r} - R_{r,f}\right)}{L} \tag{29}$$

wherein T_f, NT_f, $R_{r,f}$ and T_r, NT_r, $R_{r,r}$ are, in order, the total driving torque, net traction and rolling radius of the front and rear wheel respectively; h is the height of the drawbar measured on the field in the operating configuration, and L is the wheelbase of the tractor.

Equation 29 is derived by assuming that the rolling radius is a good approximation of the height of the wheel hub and is constant, and the rut depth is small enough to be neglected in the calculation. The system of Equations 27, 28 and 29 is valid when the pulling force is applied horizontally, which means that the total tractor weight remains constant, with only its distribution changing between the front and rear axles.

For a MFWD tractor with rigid coupling between the front and the rear axles, the ratio of the theoretical speed of the front wheel to that of the rear wheel K_s is fixed, and hence there is a precise relationship between the slip of the front wheel i_{front} and that of the rear wheel i_{rear} in straight line motion:

$$i_{front} = 1 - \frac{\left(1 - i_{rear}\right)}{K_s} \tag{30}$$

Preliminary tests with the MFWD 65 kW tractor in the four configurations considered have indicated values of K_s very close to 1 with a minimum of 0.993 and a maximum of 1.002, allowing a simplified analysis in which the slip of the front and rear wheels are assumed to be the same.

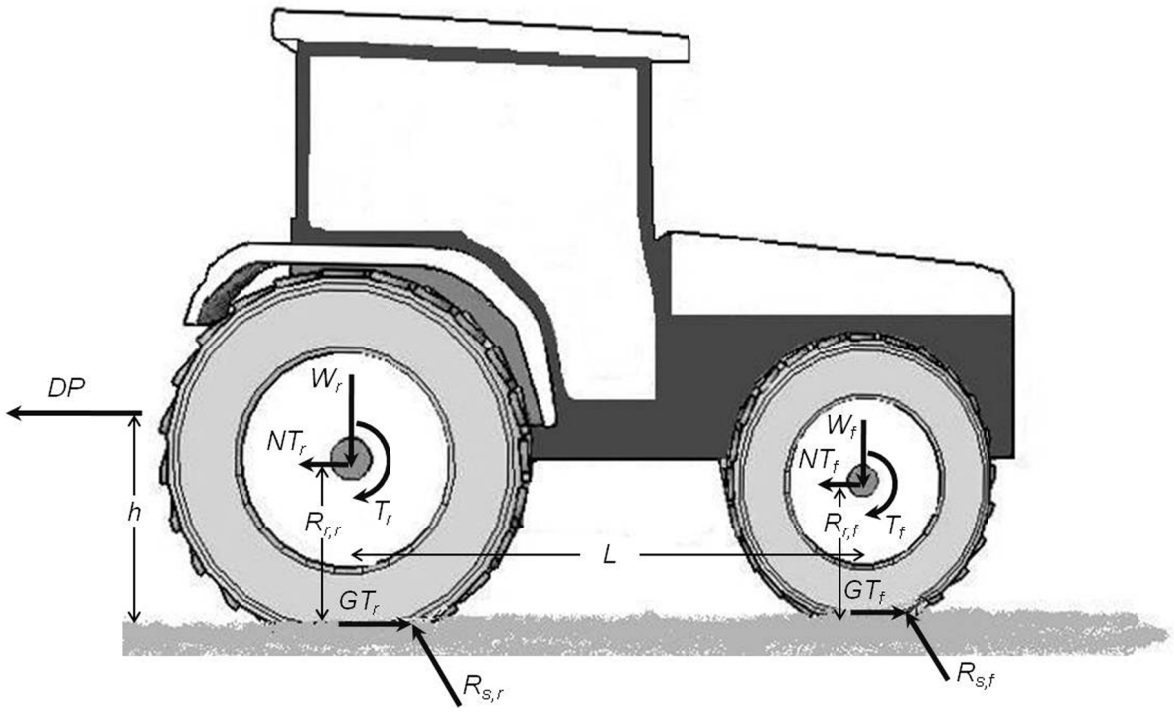

Figure 2. Forces on a MFWD tractor

The model described was written in a Visual Basic code. The main steps in the calculation of traction performance are reported in the flowchart in Figure 3. The calculation procedure can be divided into two main steps: the first defines the soil-tyre contact surface and the second calculates the traction performance in terms of gross traction, soil compaction resistance, net traction, and total driving torque. Since a variation in slip in the range considered causes the tractor weight to be distributed differently between the front and the rear axles, the calculation is repeated until a defined $slip_f$ value is reached. The traction performance of the tractor-soil system is given by the sum of the traction performances obtained for the two axles.

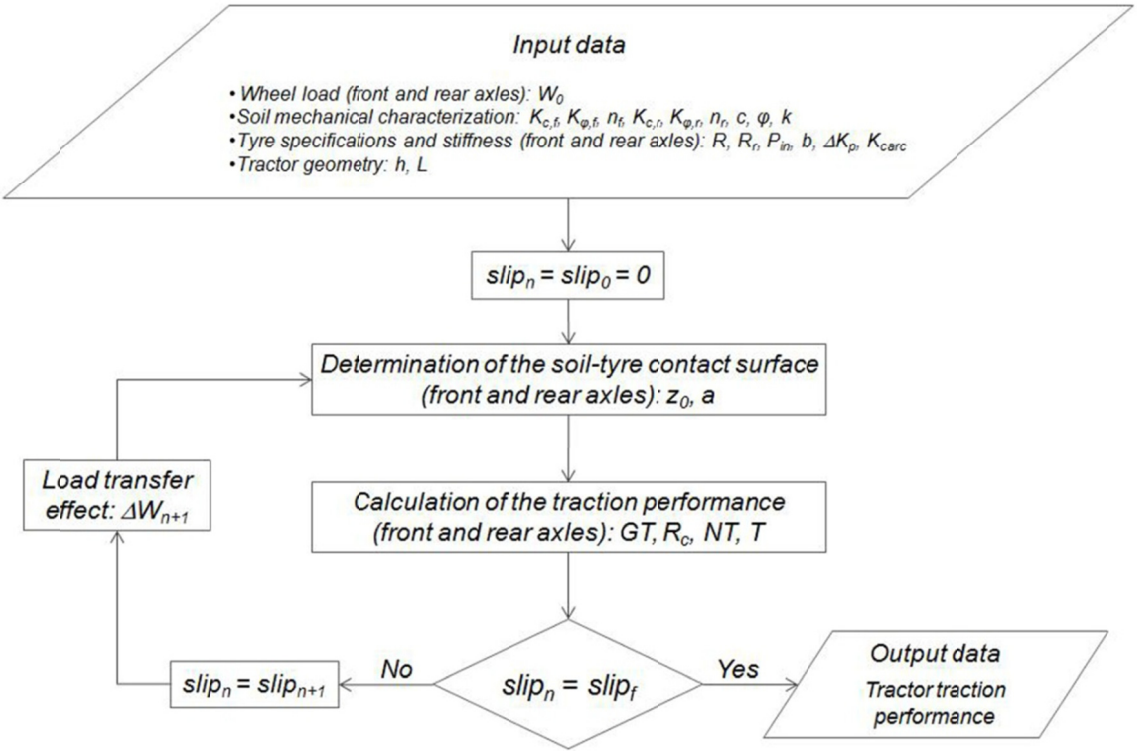

Figure 3. Flowchart of the calculation procedure for tractor traction performance

2.3 Design of Traction Tests

The traction tests took place in a flat agricultural field of clay (C) Vertic Cambisol in Ettenhausen, Switzerland [47°28'52"N, 8°54'14"E].

Corridors 4 m wide and 70 m long were marked out in the field. The corridors were navigated in steady-state motion, controlling the drawbar pull developed by the pulling tractor with a braking tractor used as a dynamometer. Drawbar pull was varied from one corridor to the next, as was, therefore, the slip, which ranged between 6% and 28%. The layout of the traction test in steady-state motion along a corridor is sketched in Figure 4.

A 200 kN load cell (HBM U2B, Darmstadt, Germany) was used to measure drawbar pull. Actual forward velocity was measured by a radar velocity sensor (DICKEY-john RVS2, Auburn, Illinois, USA), whilst the wheel rolling velocity was recorded via a wireless wheel speed sensor (two pulses per wheel revolution) set on a rear wheel of the pulling tractor. An automatic acquisition system in the braking tractor recorded and displayed all these parameters.

In order to measure fuel consumption, the pulling tractor was fitted with an external fuel tank and a switch for changing between the internal and external fuel tanks. Fuel consumption was measured as the difference in weight of the external fuel tank before and after driving along a corridor.

The pulling tractor moved in a rectilinear direction with locked differential, which allowed the highest traction performance to be achieved. During the tests, engine speed was kept at a constant 1700 rpm (68% rated speed) by means of the hand throttle. This engine speed corresponded to the highest torque and the lowest specific fuel

consumption of the engine. Two different gears were used in order to maximise the drawbar power developed: 1S at low slip and drawbar pull, and 4N at high slip and drawbar pull.

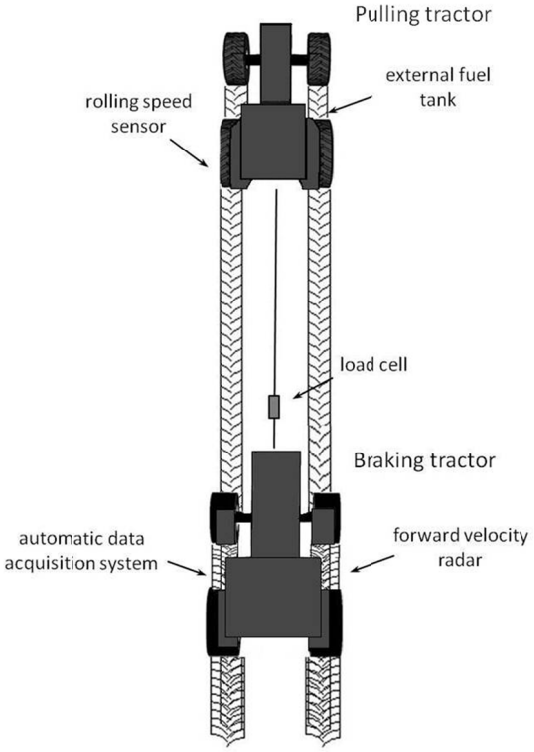

Figure 4. Layout of the traction test

2.4 Characteristics of the Tractors

The specifications of the tractors used in the traction tests are reported in Table 1.

The pulling tractor was a MFWD Hürlimann H488 DT 65 kW weighing 40.8 kN, whilst the braking tractor was a John Deere 6920 weighing 66.7 kN. The pulling tractor was equipped with 380/85R24 front tyres and 420/85R34 rear tyres.

Table 1. Some specifications of the tractors used in the traction performance studies

Braking tractor	John Deere 6920 (110 kW)			
Weight (kN)	66.7			
Pulling tractor	Hürlimann H488 DT (65 kW)			
Weight (kN)	40.8			
Wheelbase L (m)	2.34			
Tyre (front - rear)	380/85R24 - 420/85R34			
Tyre width b (front - rear) (m)	0.38 - 0.44			
Tyre unloaded radius R (front - rear) (m)	0.63 - 0.79			
Rim diameter D_{rim} (front - rear) (m)	0.61 - 0.86			
Tyre carcass stiffness K_{carc} (front - rear) (kN m^{-1})	129.5 - 111.8			
Pressure dependence of tyre ΔK_p (front - rear) (kN m^{-1} kPa^{-1})	1.22 - 2.00			
	L1P1	L1P2	L2P1	L2P2
Height of the drawbar h (m)	0.80	0.83	0.71	0.77
Stationary wheel load W_0 (front - rear) (kN)	9.3 - 11.1	9.3 - 11.1	10.5 - 14.6	10.5 - 14.6
Tyre rolling radius R_r (front - rear) (m)	0.58 - 0.76	0.59 - 0.77	0.58 - 0.76	0.58 - 0.77
Tyre inflation pressure P_{in} (front - rear) (kPa)	60 - 60	160 - 160	60 - 60	160 - 160
Tyre stiffness (front - rear) (kN m^{-1})	203 - 232	325 - 432	203 - 232	325 - 432

Traction performance was measured in four configurations (L1P1, L1P2, L2P1, L2P2) in which tractor weight was varied between 40.8 kN and 50.2 kN with ballasts, and tyre inflation pressure was varied between 60 kPa and 160 kPa (Table 1). The wheel load and tyre pressure values considered are representative for medium powered tractors, and were matched according to the indications of the tyre manufacturer. The load acting on the wheels in the stationary condition was measured with a flat bed wheel load scale (Haenni WL 103, Jegenstorf, Switzerland). Tyre inflation pressure was measured with a Motometer tyre pressure gauge (Mühlacker-Lomersheim, Germany).

The tyre rolling radius R_r (Table 1) was determined according to American Society of Agricultural Engineers (ASAE) Standard S296.2 as the distance travelled per revolution of the wheel divided by 2π when operating at the specified zero condition. The latter was here assumed to be the vehicle operating at zero drawbar pull on a smooth road. This condition allows the travel reduction (slip) to have a fixed base which is not dependent upon the test condition (soil strength) (Wismer & Luth, 1973). Moreover, the difference in measured rolling radii between a hard surface and a test surface is small under normal agricultural soil conditions (untilled soil), and thus has little impact on the final results (Zoz & Grisso, 2003). A significant linear type regression between the rolling radius of the front and rear wheels and the inflation pressure at the two wheel loads considered is shown in Figure 5.

Parameters K_{carc} and ΔK_p (Table 1), which characterise tyre stiffness, were determined on the basis of the tyre specifications as in Lines and Murphy (1991).

The relationship between *PTO* (power-take-off) and fuel consumption in kg/h at 1700 rpm engine speed (Figure 6) was derived in a laboratory test with a torque dynamometer (Schenck W700, Darmstadt, Germany).

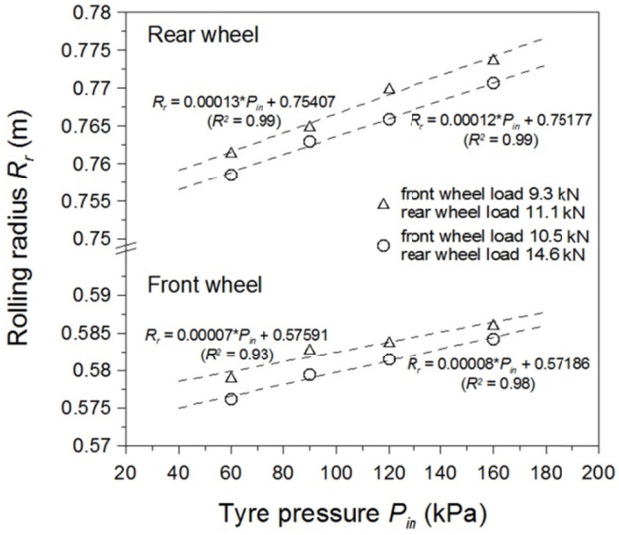

Figure 5. Variation of the rolling radius of the front wheel (380 85R24 tyre) and the rear wheel (420 85R34 tyre) with the inflation pressure at two wheel loads

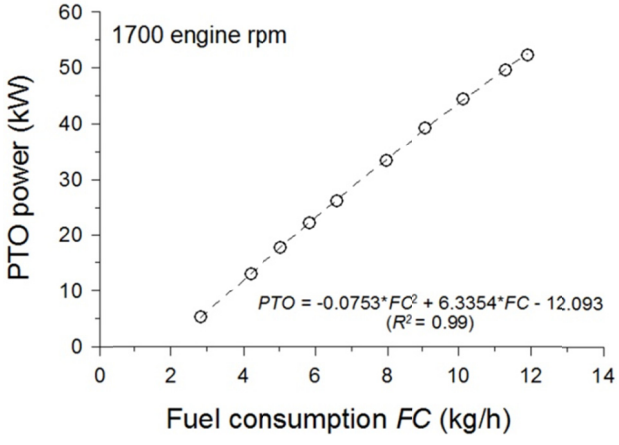

Figure 6. Ratio between PTO and fuel consumption of the Hürlimann H488 DT 65 kW at 1700 rpm engine speed

2.5 Characteristics of the Topsoil

Some physical parameters of the agricultural clay (C) Vertic Cambisol are listed in Table 2, along with the mechanical parameters for the soil-tyre interaction model.

Soil texture was characterised according to the United States Department of Agriculture (USDA) classification system, moreover, soil type was classified according to the Food and Agriculture Organization of the United Nations (FAO) system (2006). Bulk density was measured on undisturbed soil samples according to Blake and Hartge (1986). Volumetric water content was measured via a time domain reflectometry (TDR) device (E.S.I. Environmental sensors MP-917, Sidney, Canada) with two-rod single diode probes.

Topsoil mechanical parameters for the soil-tyre interaction model were derived via vertical plate penetration tests and horizontal plate shear deformation tests with a tractor-mounted bevameter (Bekker, 1960). An exhaustive description of the bevameter used was given by Diserens and Steinmann (2003).

Vertical plate penetration tests were carried out with two circular plates of 20 cm and 30 cm diameter at a penetration rate of around 0.02 m s^{-1}. The cohesive and frictional moduli of deformation K_c and K_φ as well as the exponent of deformation n were determined according to Wong (1980). The horizontal plate shear deformation tests were performed by an annular plate with an outer diameter of 30 cm and an inner diameter of 20 cm at different vertical pressures ranging between 25 and 215 kPa. Measured shear stress-displacement curves were fitted with equation 15, and values of c, φ and k were determined according to the procedure described by Wong (1980).

In order to consider the multipass effect, i.e. the different behaviour of soil interacting with the front and rear wheel, the vertical plate penetration tests and the horizontal plate shear deformation tests were performed before the passage of the tractor, as well as on the rut left by the passage of the front wheel. Because the parameters K_c, K_φ and n calculated before and after the passage of the front wheel changed significantly, they were differentiated for soil interacting with the front wheel ($K_{c,f}$, $K_{\varphi,f}$, n_f) and soil interacting with the rear wheel ($K_{c,r}$, $K_{\varphi,r}$, n_r), as reported in Table 2. A unique characterization was adopted for shear parameters c, φ and k, as they did not change significantly before and after the passage of the front wheel (Table 2).

Table 2. Some characteristics of the clay soil used in the traction performance studies

Soil property	0-0.20 m depth
Sand (g kg^{-1})	200
Silt (g kg^{-1})	320
Clay (g kg^{-1})	480
Texture (USDA classification)	Clay (C)
Soil classification (FAO, 2006)	Vertic Cambisol
Dry bulk density (Mg m^{-3})	1.31
Volumetric water content (%)	27.0
Cohesive modulus of deformation (front wheel) $K_{c,f}$ (kN $m^{-(n+1)}$)	2354.1
Frictional modulus of deformation (front wheel) $K_{\varphi,f}$ (kN $m^{-(n+2)}$)	-4130.0
Exponent of deformation (front wheel) n_f	1.01
Cohesive modulus of deformation (rear wheel) $K_{c,r}$ (kN $m^{-(n+1)}$)	2168.9
Frictional modulus of deformation (rear wheel) $K_{\varphi,r}$ (kN $m^{-(n+2)}$)	-3498.3
Exponent of deformation (rear wheel) n_r	0.79
Cohesion c (kPa)	24.4
Angle of shear resistance φ (°)	18.0
Shear deformation modulus k (m)	0.014

3. Results

3.1 Simulation of Contact Surface and Contact Stresses

The reliability of the soil-tyre interaction model for simulating both wheel sinkage (rut depth) and traction performance was pointed out by Osetinsky and Shmulevich (2004).

The simulation of the soil-tyre contact surface and the contact stresses (normal σ and shear τ) together with the soil

strength τ_{max} for the rear wheel at a slip of 10% in the four cases considered, is represented in Figure 7. Soil strength is given by:

$$\tau_{max} = \left(c + \sigma tan\varphi\right) \tag{31}$$

the latter corresponds to the horizontal asymptote of equation 15 and defines the maximum shear stress on soil under a given normal stress.

The geometry of the soil-tyre contact surface is defined by the *x*-axis and the *z*-axis according to the reference system in Figure 1. The stress condition at the soil-tyre contact together with the soil strength is defined by the *x*-axis and the Stress-axis.

The geometry of the contact surface as well as the contact stresses and soil strength varied more noticeably with the increase in tyre pressure than with the increase in wheel load, with the former producing a deeper and shorter contact surface, and the latter creating a deeper and longer one.

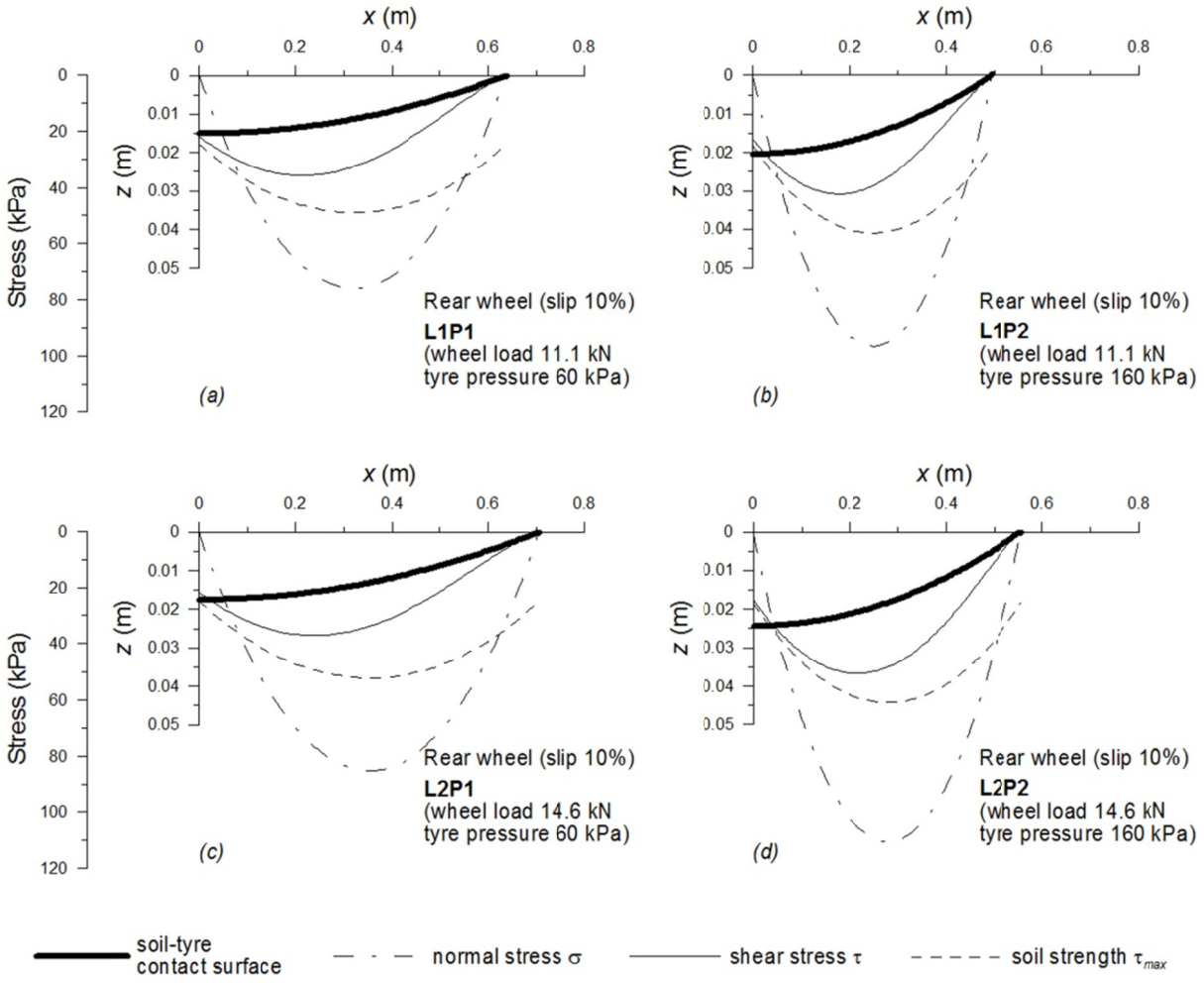

Figure 7. Simulation of the geometry of the soil-tyre contact surface, the contact stresses (normal σ and shear τ), and the soil strength τ_{max} for the rear wheel (420 85R34 tyre) at a slip of 10% in the four configurations considered

3.2 Measurement and Simulation of Drawbar Pull and Traction Coefficient

The measured and simulated traction performance in terms of drawbar pull *DP* and traction coefficient μ_{tr} as a function of slip *i* are reported in Figure 8.

Lowering the inflation pressure produced an improvement in drawbar pull and traction coefficient both with and without ballasting the tractor.

The increase in wheel load resulted in a higher drawbar pull at both 60 kPa and 160 kPa tyre inflation pressure, although it failed to produce noteworthy variations in terms of traction coefficient.

Figure 9 shows the simulation of the traction coefficient as a function of slip (from 4% to 25%) and tyre inflation pressure (from 60 to 160 kPa) both without (Figure 9*a*) and with ballasts (Figure 9*b*). In this simulation, the slip base is assumed to vary according to the variation of the rolling radius reported in Figure 5.

Tyre pressure had a significant effect on traction coefficient, which decreased with increasing pressure. The increase in tractor weight (wheel load) resulted in a slight decrease in traction coefficient.

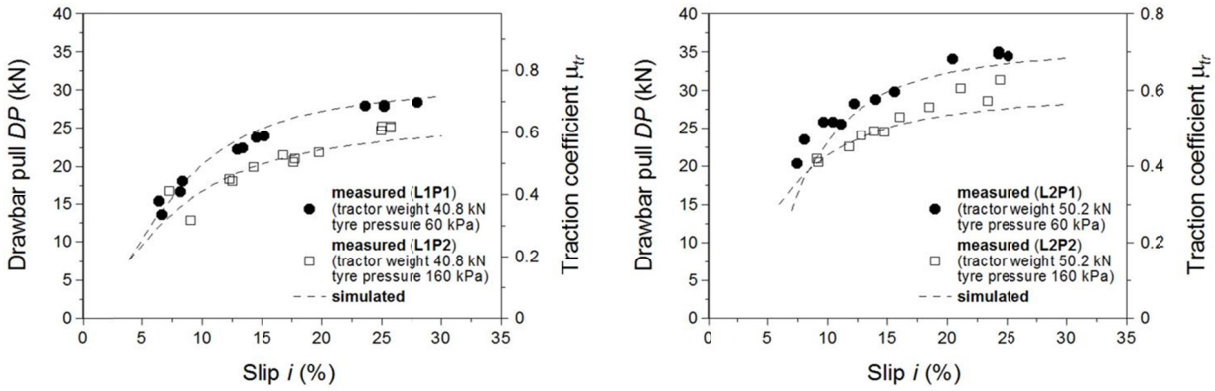

Figure 8. Measured and simulated drawbar pull and traction coefficient as a function of slip in the four configurations considered

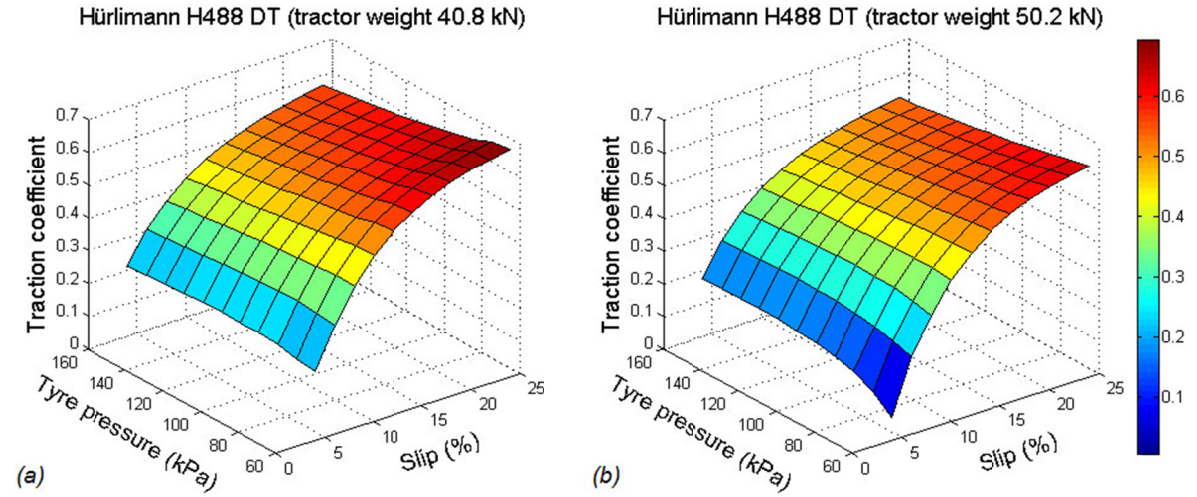

Figure 9. Simulation of the traction coefficient as a function of slip (from 4% to 25%) and tyre inflation pressure (from 60 to 160 kPa) without ballasts *(a)* and with ballasts *(b)*

3.3 Simulation of Tractive Efficiency

In order to properly measure the tractive efficiency η_{tr}, a wheel torque dynamometer - not available for our tests - would be required. Tractive efficiency was therefore merely simulated as a function of slip (from 4% to 25%) and tyre inflation pressure (from 60 to 160 kPa) without ballasts (Figure 10*a*) and with ballasts (Figure 10*b*).

It emerged that tractive efficiency decreased along with an increase in both tyre pressure and wheel load, although the decrease owing to wheel load was less significant.

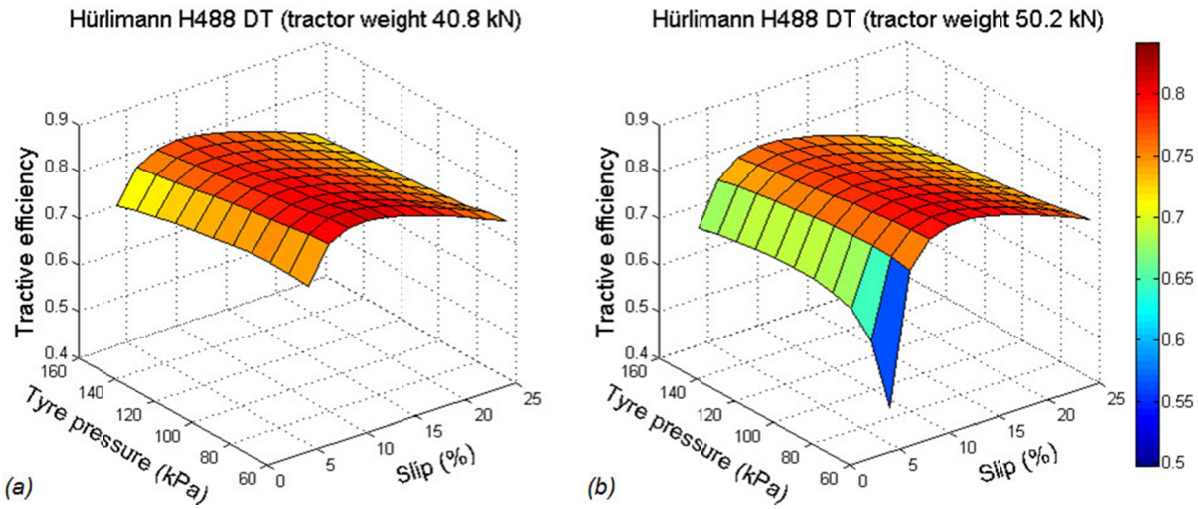

Figure 10. Simulation of tractive efficiency as a function of slip (from 4% to 25%) and tyre inflation pressure (from 60 to 160 kPa) without ballasts *(a)* and with ballasts *(b)*

3.4 Measurement and Fitting of Power Delivery Efficiency and Specific Fuel Consumption

Values for power delivery efficiency η_{PD} and specific fuel consumption *SFC* (drawbar power basis) as a function of the slip are reported in Figure 11 for the four tractor configurations considered (Table 1). The equivalent *PTO* was calculated on the basis of measured fuel consumption, according to Figure 6.

Power delivery efficiency and specific fuel consumption were fitted (least squares method) with the following equations:

$$\eta_{PD} = Ae^{\left(1-\frac{i}{l_A}\right)}\left(\frac{i}{l_A}\right)^{\left(1+\theta_A\frac{i}{l_A}\right)} \tag{32}$$

and

$$SFC = \frac{1}{Be^{\left(1-\frac{i}{l_B}\right)}\left(\frac{i}{l_B}\right)^{\left(1+\theta_B\frac{i}{l_B}\right)}} \tag{33}$$

wherein A, l_A, θ_A and B, l_B, θ_B are fitting parameters which mainly control: the positive peak of η_{PD} (parameter A), the negative peak of *SFC* (parameter B), the slip value at which the peak is reached (parameters l_A and l_B), and the slope of the curve beyond the peak (parameters θ_A and θ_B). Values of these parameters as well as the root mean square error *RMSE* of the fitting are reported in Table 3.

An increase in tyre pressure resulted in lower power delivery efficiency and higher specific fuel consumption at both tractor weights, with a more significant variation at a tyre pressure of 60 kPa.

An increase in tractor weight, at least at a slip of less than 15%, resulted in a notable decrease in power delivery efficiency and an increase in specific fuel consumption at a tyre pressure of 60 kPa, as well as a slight decrease in power delivery efficiency with a more significant decrease in specific fuel consumption at a tyre pressure of 160 kPa.

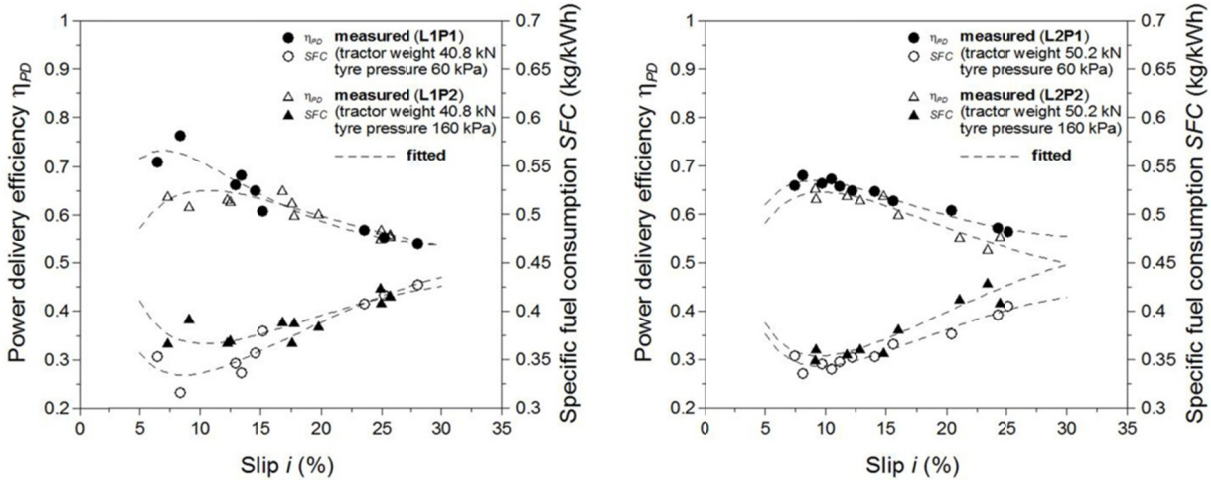

Figure 11. Measured and fitted power delivery efficiency and specific fuel consumption (drawbar power basis) as a function of slip in the four configurations considered

Table 3. Values of parameters A, l_A, θ_A and B, l_B, θ_B, and root mean square error *RMSE* from the fitting of the power delivery efficiency η_{PD} and the specific fuel consumption *SFC*

	η_{PD}				*SFC*			
	A	l_A	θ_A	*RMSE*	B	l_B	θ_B	*RMSE*
	-	-	-	-	(kW h kg^{-1})	-	-	(kg kW^{-1} h^{-1})
L1P1	0.67	3.77	0.28	0.019	2.74	4.62	0.28	0.011
L1P2	0.59	5.98	0.29	0.016	2.47	5.26	0.29	0.010
L2P1	0.61	4.68	0.29	0.007	2.65	4.94	0.29	0.005
L2P2	0.60	5.98	0.27	0.012	2.59	5.08	0.28	0.009

4. Discussion

The advantages in decreasing tyre inflation pressure or ballasting the tractor may be greater or lesser, depending on the change in the interaction between soil and tyre.

It emerged that the traction performance of the tractor considered (Table 1) depended on the geometry of the contact surface between tyre and soil, as well as on contact stresses and soil strength (Figure 7). All of these factors varied significantly with the inflation pressure, and less noticeably with the stationary wheel load in the four configurations considered (Figure 7).

At low inflation pressure (Figures 7*a* and 7*c*), the simulated contact surface was shallow and long. This implied, on the one hand, low soil strength due to low contact pressure, as well as high rolling resistance due to high tyre deformation, and on the other hand, low soil compaction resistance due to low soil sinkage, and the soil strength used on a more extended surface.

According to equation 31, soil strength is given by a cohesive component c and a frictional component $\sigma tan\varphi$ which depends on the normal stress σ. When the inflation pressure was reduced at constant wheel load, the improvement in traction performance was mainly due to the mobilisation of the cohesive component of the soil strength on a more extended contact area, i.e. a higher total contribution of the cohesive component of the soil strength along the contact surface. This allowed better use of the soil strength, which for the same slip resulted in a higher drawbar pull and traction coefficient (Figures 8 and 9), higher simulated tractive efficiency (Figure 10), higher power delivery efficiency, and lower specific fuel consumption (Figure 11).

When the stationary wheel load was increased at a constant tyre pressure, the simulated contact surface varied slightly, becoming longer and deeper (Figures 7*a* and 7*c* and Figures 7*b* and 7*d*). This implied, on the one hand, higher rolling resistance due to greater tyre deformation and higher soil compaction resistance due to greater soil sinkage, and on the other hand, higher soil strength due to greater normal contact stress and the soil strength used on a more extended surface. The improvement of traction performance in terms of drawbar pull (Figure 8) was

partly due to a higher total contribution of the frictional component of the soil strength and partly due to a higher total contribution of the cohesive component of the soil strength along the contact surface. In spite of the higher drawbar pull, this way of using the soil strength did not result in any improvement in terms of traction coefficient (Figures 8 and 9), simulated tractive efficiency (Figure 10), or power delivery efficiency (Figure 11). At a slip of under 15%, only the specific fuel consumption decreased with increasing wheel load at a tyre pressure of 160 kPa.

The results of this study may provide helpful indications for an appropriate choice of tractor configuration on cohesive soils in order to optimise tractor performance, thereby saving time and reducing the costs of tillage management.

5. Conclusions

The present study aimed to analyse the effects of variations in tyre inflation pressure and wheel load on the traction performance of a 65 kW MFWD tractor on an agricultural clay (C) Vertic Cambisol.

In the conditions examined, although the tractor developed higher drawbar pull both when tyre inflation pressure was decreased and wheel load was increased, only the decrease in tyre pressure produced improvements in terms of coefficient of traction, tractive efficiency, power delivery efficiency, and specific fuel consumption, while the only significant benefit due to the increase in wheel load was a reduction in the specific fuel consumption at a tyre pressure of 160 kPa and a slip of under 15%. A mechanistic interpretation of these results was proposed.

Two equations describing the relationships power delivery efficiency-wheel slip and specific fuel consumption-wheel slip were presented.

The results of this study may provide helpful indications for an appropriate choice of tractor configuration, as well as for the reasonable control of wheel slip, with a view to optimising traction performance on cohesive soils, thereby saving time and reducing the costs of tillage management.

Acknowledgements

We wish to acknowledge the Swiss Federal Office for the Environment FOEN and the tyre manufacturer Michelin for providing the financial support for this study.

Our thanks go to Beat Kürsteiner, Jakob Heusser and Isidor Schiess for their technical assistance. We also would like to thank Marco Landis for providing data reported in Figure 6.

References

American Society of Agricultural Engineers. (1983). *Agricultural engineers yearbook of standards*. ASAE Standard S296.2 - Uniform terminology for traction of Agricultural Tractors, Self-Propelled Implements, and other Traction and Transport Devices. St. Joseph, Mich.: ASAE.

Bekker, M. G. (1960). *Off-the-Road Locomotion*. Ann Arbor, Mich., University of Michigan Press.

Blake, G. R., & Hartge, K. H. (1986). Bulk density - Core method. In: Klute A. (Ed.), Methods of Soil Analysis, Part 1. *Physical and Mineralogical Methods* (pp. 364-367) - Agronomy Monograph no. 9 (2nd Edition). American Society of Agronomy - Soil Science Society of America, Madison, Wisconsin.

Burt, E. C., Bailey, A. C., Patterson, R. M., & Taylor, J. H. (1979). Combined effects of dynamic load and travel reduction on tire performance. *Trans. ASAE, 22*(1), 40-45.

Burt, E. C., & Bailey, A. C. (1982). Load and inflation pressure effects on tires. *Trans. ASAE, 25*(4), 881-884.

Burt, E. C., Lyne, P. W. L., Meiring, P., & Keen, J. F. (1983). Ballast and inflation effects on tire efficiency. *Trans. ASAE, 26*, 1352-1354.

Charles, S. M. (1984). Effects of ballast and inflation pressure on tractor tire performance. *Agricultural engineering, 65*(2), 11-13.

Food and Agriculture Organization. (2006). *World reference base for soil resources*. Report No. 103, Rome, Italy.

Fujimoto, Y. (1977). Performance of elastic wheels on yielding cohesive soils. *J. Terramech., 14*(4), 191-210. http://dx.doi.org/10.1016/0022-4898(77)90034-9

Gee-Clough, D., McAllister, M., & Evernden, D. W. (1977). Tractive performance of tractor drive tyres II. A comparison of radial and cross-ply carcass construction. *J. agric. Engng Res., 22*, 385-395. http://dx.doi.org/10.1016/0021-8634(77)90069-5.

Gee-Clough, D., Pearson, G., & McAllister, M. (1982). Ballasting wheeled tractors to achieve maximum power output in frictional-cohesive soils. *J. agric. Engng Res., 27*, 1-19. http://dx.doi.org/10.1016/0021-8634(82)90053-1.

Janosi, Z., & Hanamoto, B. (1961). The analytical determination of drawbar pull as a function of slip for tracked vehicles in deformable soils. In: *Proceedings of the 1st International Conference on the Mechanics of Soil-Vehicle Systems* (pp. 707-736). Edizioni Minerva Tecnica, Torino, Italy.

Jenane, C., Bashford, L. L., & Monroe, G. (1996). Reduction of fuel consumption through improved tractive performance. *J. agric. Engng Res., 64*, 131-138. http://dx.doi.org/10.1006/jaer.1996.0054.

Lee, D. R., & Kim, K. U. (1997). Effect of inflation pressure on tractive performance of bias-ply tires. *J. Terramech., 34*(3), 187-208. http://dx.doi.org/10.1016/S0022-4898(97)00033-5.

Lines, J. A., & Murphy, K. (1991). The stiffness of agricultural tractor tyres. *J. Terramech., 28*(1), 49-64. http://dx.doi.org/10.1016/0022-4898(91)90006-R.

Lyne, P. W. L., Burt, E. C., & Meiring, P. (1984). Effect of tire and engine parameters on efficiency. *Trans. ASAE, 27*(1), 5-7.

Osetinsky, A., & Shmulevich, I. (2004). Traction performance simulation of a pushed/pulled driven wheel. *Trans. ASAE, 47*(4), 981-994.

Schmid, I. C. (1995). Interaction of vehicle and terrain results from 10 years research at IKK. *J. Terramech., 32*(1), 3-26. http://dx.doi.org/10.1016/0022-4898(95)00005-L

Serrano, J. M., Peça, J. O., Silva, J. R., & Márquez, L. (2009). The effect of liquid ballast and tyre inflation pressure on tractor performance. *Biosyst. Eng., 102*, 51-62. http://dx.doi.org/10.1016/j.biosystemseng.2008.10.001.

Servadio, P. (2010). Applications of empirical methods in central Italy for predicting field wheeled and tracked vehicle performance. *Soil Till. Res., 110,* 236-242. http://dx.doi.org/10.1016/j.still.2010.08.009

Shell, L. R., Zoz, F. M., & Turner, R. L. (1997). Field performance of rubber belt and MFWD tractors in Texas soils. In: *Belt and Tire Traction in Agricultural Vehicles,* (SP-1291), 65-73. SAE technical paper series 972729. SAE.

Shmulevich, I., & Osetinsky, A. (2003). Traction performance of a pushed/pulled drive wheel. *J. Terramech., 40*, 35-50. http://dx.doi.org/10.1016/j.jterra.2003.09.001.

Turner, R. J. (1993). A simple system for determining tractive performance in the field. *ASAE/CSAE meeting presentation*, *ASAE paper No. 93-1574*. St. Joseph, Mich.: ASAE.

Turner, R. J., Shell, L. R., & Zoz, F. M. (1997). Field performance of rubber belt and MFWD tractors in southern Alberta soils. In: *Belt and Tire Traction in Agricultural Vehicles,* (SP-1291), 75-85. SAE technical paper series 972730. SAE.

Wismer, R. D., & Luth, H. J. (1973). Off-road traction prediction for wheeled vehicles. *J. Terramech., 10*(2), 49-61. http://dx.doi.org/10.1016/0022-4898(73)90014-1

Wong, J. Y., & Reece, A. R. (1967). Prediction of rigid wheel performance based on the analysis of soil-wheel stresses, part I. Performance of driven rigid wheels. *J. Terramech., 4*(1), 81-98. http://dx.doi.org/10.1016/0022-4898(67)90105-X

Wong, J. Y. (1980). Data processing methodology in the characterization of the mechanical properties of terrain. *J. Terramech., 17*(1), 13-41. http://dx.doi.org/10.1016/0022-4898(80)90014-2

Wong, J. Y. (1989). *Terramechanics and off-road vehicles*. The Netherlands: Elsevier Science, Amsterdam.

Wong, J. Y. (2008). *Theory of Ground Vehicles.* John Wiley and Sons, Hoboken, New Jersey.

Zombori, J. (1967). Drawbar pull tests of various traction devices on sandy soils. *J. Terramech., 4*(1), 9-17. http://dx.doi.org/10.1016/0022-4898(67)90100-0

Zoz, F. M., Turner, R. J., & Shell, L. R. (2002). Power delivery efficiency: a valid measure of belt and tire tractor performance. *Trans. ASAE, 45*(3), 509-518.

Zoz, F. M., & Grisso, R. D. (2003). Traction and tractor performance. *ASAE distinguished lecture series (Tractor design No. 27)*. ASAE publication No. 913C0403. St. Joseph, Mich.: ASAE.